JOC*Article*

# Theoretical and Experimental Studies of Asymmetric Organozinc Additions to Benzaldehyde Catalyzed by Flexible and Constrained γ-Amino Alcohols

Manoranjan Panda, Puay-Wah Phuan, and Marisa C. Kozlowski*

*Department of Chemistry, Roy and Diana Vagelos Laboratories, University of Pennsylvania, Philadelphia, Pennsylvania 19104*

*marisa@sas.upenn.edu*

*Received July 20, 2002*

The *cis*-decalin based γ-amino alcohols, **1**−**5**, were synthesized, resolved, and employed as catalysts in the addition of organozincs to benzaldehyde. Despite large facial differentiation in the RZn adducts of the ligands, the enantioselectivities were found to be moderate. Transition structure calculations were done using several quantum chemical methods to examine the underlying causes of the selectivity for three γ-amino alcohols, **1**, **2**, and **3**. The tricyclic μ-oxo (6/4/4), rather than the bicyclic six-membered (6/6), transition structures were found to explain the observed enantioselectivity for **2** and **3**. MP2 calculations gave the best correlation to the experimental results compared to B3LYP and HF calculations. The conformational flexibility of the chiral ligands was found to be an important factor in the selectivity.

## Introduction

The identification of new chiral ligands for asymmetric synthesis remains an important endeavor. Using a database mining protocol to find novel ligand architectures,[1] we have identified the *cis*-decalin architecture as potentially useful (Figure 1).

*cis*-Decalins provide a flexible framework for the construction of a wide variety of interesting chiral ligands including diamines,[2] diols, amino alcohols, phosphites, and phosphines. Several examples of non-$C_2$-symmetric γ-amino alcohols based upon the *cis*-decalin skeleton can be imagined (Figure 2). In this study, the utility of *cis*-decalin derivatives **1** and **2** was investigated in the asymmetric addition of organozincs to aldehydes on the basis of PM3 transition structure calculations which predicted high levels of enantioselectivity for **2**. Further constrained analogues of **2** (**3**−**5**) were also prepared and examined in order to determine the role of conformational flexibility on the selectivities of **1** and **2**.

The discovery that chiral amino alcohols, such as DAIB, are excellent catalysts for the enantioselective addition of dialkylzincs to aldehydes[3,4] has stimulated a host of efforts directed at understanding the mechanism, stereochemical induction, and scope of this reaction. Due to its relative simplicity, this reaction is also an ideal case for addressing the necessary architectures and elements required for high stereochemical induction. β-Amino alcohols have typically been employed in this reaction although a number of γ-amino alcohols[3b,5] have also been used successfully.

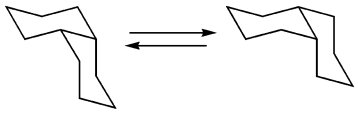

**FIGURE 1.** *cis*-Decalin.

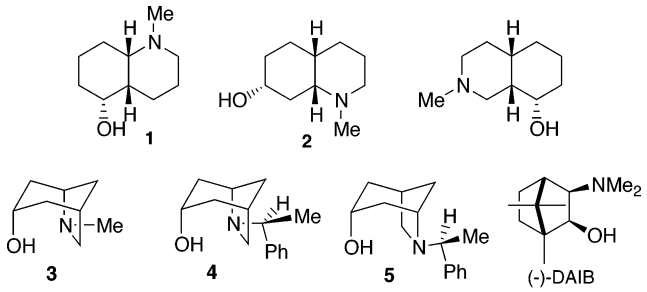


**FIGURE 2.** *cis*-Decalin γ-amino alcohols, constrained analogues, and DAIB.

Rationalizations of the observed stereoselectivity of asymmetric dialkylzinc additions to benzaldehyde catalyzed by amino alcohols have been reported by various research groups utilizing transition structure analyses.[6] However, there is sparse information regarding the theoretical investigation of the reaction with γ-amino alcohol catalysts. We wished to determine if the reported

(1) Kozlowski, M. C.; Panda, M. *J. Mol. Graphics Modell.* **2002**, *20*, 399.

(2) (a) Li, X.; Schenkel, L. B.; Kozlowski, M. C. *Org. Lett.* **2000**, *2*, 875. (b) Li, X.; Yang, J.; Kozlowski, M. C. *Org. Lett.* **2001**, *3*, 1137.

(3) For reviews, see: (a) Soai, K.; Niwa, S. *Chem. Rev.* **1992**, *92*, 833. (b) Noyori, R. In *Asymmetric Catalysis In Organic Synthesis*; John Wiley & Sons: New York, 1994; p 260.

(4) Pu, L.; Yu, H.-B. *Chem. Rev.* **2001**, *101*, 757.

(5) Some examples of γ-amino alcohols used in organozinc alkylation: (a) Oppolzer, W.; Radinov, R. N. *Tetrahedron Lett.* **1988**, *29*, 5645. (b) Muchow, G.; Vannoorenberghe, G.; Buono, G. *Tetrahedron Lett.* **1987**, *28*, 6163. (c) Cho, B. T.; Kim, N. *Tetrahedron Lett.* **1994**, *35*, 4115. (d) Hulst, R.; Heres, H.; Fitzpatrick, K.; Peper, N.; Kellogg, R. M. *Tetrahedron: Asymmetry* **1996**, *7*, 2755. (e) Cicchi, S.; Crea, S.; Goti, A.; Brandi, A. *Tetrahedron: Asymmetry* **1997**, *8*, 293.

10.1021/jo0262210 CCC: $25.00 
Published on Web 12/24/2002

**SCHEME 1**

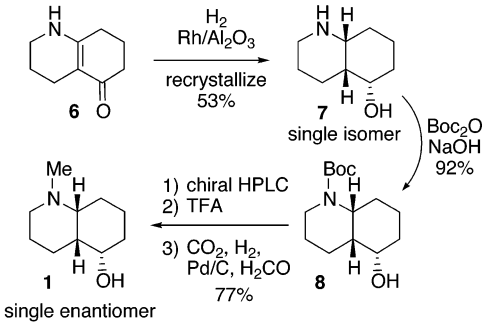


analyses were reliable in predicting selectivity for this slightly different ligand type. In this report, we compare a theoretical evaluation of *cis*-decalin $\gamma$-amino alcohols in this reaction with the experimental results.

## Results and Discussion

**Synthesis of *cis*-Decalin $\gamma$-Amino Alcohols 1 and 2.** Several syntheses of the basic structure found in **1** have been reported.[7] A modified approach was developed as shown in Scheme 1 which was amenable to large scale synthesis and provided **1** in high yield using simple transformations. The application of $Rh/Al_2O_3$ as the hydrogenation catalyst significantly improved the yield and selectivity of the reduction of **6,** and amino alcohol **7** could be recrystallized as a single isomer. For these studies, the relatively nonpolar *N*-Boc derivative **8** was generated and then resolved using chiral HPLC. Resolved **8** could easily be converted to *N*-methyl derivative **1** by treatment with TFA followed by Eschweiler−Clarke methylation.

The synthesis of **2** was accomplished starting with ketal **10** which was generated following the method of Momose et al.[9] (Scheme 2). After the *N*-methyl amide of ketal **10** was formed, treatment with 1 N HCl yielded ketoamide **11**. Selective reduction of ketoamide **11** was accomplished using $NaBH_4$ to provide the epimeric alcohols **12α** and **12*β*** in ratio of 5:1. While **12α** and **12*β*** were not separable by silica column chromatography, the diastereomers and enantiomers of **12** could be separated with chiral HPLC. The relative stereochemistry of the desired α-epimer was secured by NOE differences unique to **12α** ($H^7$ to $H^9$). Reduction of **12α** with $LiAlH_4$ furnished **2** as an oil which could be used directly.

The absolute and relative configurations of **1** and **2** were established via anomalous dispersion from the single-crystal X-ray structures of the corresponding

**SCHEME 2**

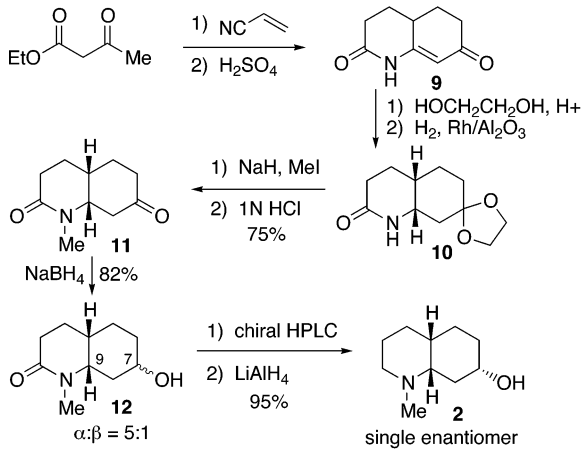


**SCHEME 3. X-ray Structures of 13 and 14 Used in Assigning the Absolute and Relative Configurations of 1 and 2**

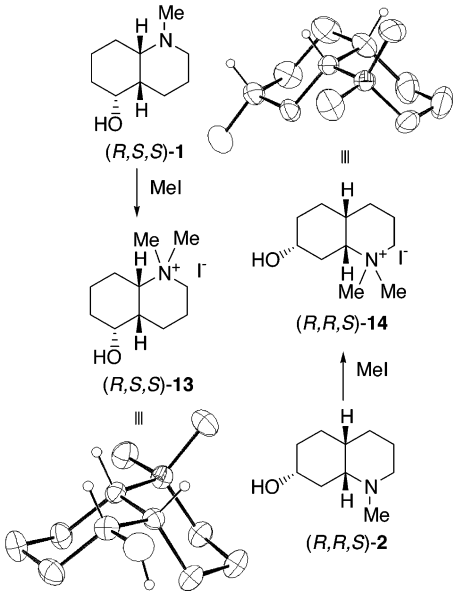


quaternary ammonium salts (Scheme 3). The salts **13** and **14** were obtained by treatment of **1** and **2**, respectively, with MeI.

**Development and Synthesis of Constrained Analogues of 2.** Since *cis*-decalin **1** and **2** are conformationally mobile, we sought to develop constrained analogues to probe the role of conformational flexibility on reactivity and selectivity. Examination of the three-dimensional structure of **2** showed that addition of a methylene would constrain the molecule (Figure 3). This constrained form contains a 6-azabicyclo[3.2.1]octane framework. Hence, amino alcohols (*S*,*S*,*R*)-**3**, (*S*,*S*,*R*,*S*)-**4**, and (*R*,*R*,*S*,*S*)-**5** were synthesized following the procedure of Carroll et al.[10] These compounds had not been examined previously as ligands in asymmetric synthesis.

**Asymmetric Organozinc Additions Catalyzed by the $\gamma$-Amino Alcohols.** On the basis of the results of PM3 transition structure calculations which predicted

(6) (a) Yamakawa, M.; Noyori, R. *J. Am. Chem. Soc.* **1995**, *117*, 6327. (b) Yamakawa, M.; Noyori, R. *Organometallics* **1999**, *18*, 128. (c) Goldfuss, B.; Houk, K. N. *J. Org. Chem.* **1998**, *63*, 8998. (d) Goldfuss, B.; Steigelmann, M.; Khan, S. I.; Houk, K. N. *J. Org. Chem.* **2000**, *65*, 77. (e) Goldfuss, B.; Steigelmann, M.; Rominger, F. *Eur. J. Org. Chem.* **2000**, 1785. (f) Goldfuss, B.; Steigelmann, M. *J. Mol. Modell.* **2000**, *6*, 166. (g) Vazquez, J.; Pericas, M. A.; Maseras, F.; Lledos, A. *J. Org. Chem.* **2000**, *65*, 7303. (h) Brandt, P.; Hedberg, C.; Lawonn, K.; Pinho, P.; Andersson, P. G. *Chem. Eur. J.* **1999**, *5*, 1692.

(7) (a) Grob, C. A.; Kiefer, H. R. *Helv. Chim.* Acta **1965**, *48*, 799. (b) Le Bel, N. A.; Caprathe, B. W. *J. Org. Chem.* **1985**, *50*, 3938. (c) Comins, D. L.; Abdullah, A. H. *Tetrahedron Lett.* **1985**, *26*, 43.

(8) Caprathe, B. W.; Jaen, J. C.; Wise, L. D.; Heffner, T. G.; Pugsley, T. A.; Meltzer, L. T.; Parvez, M. *J. Med. Chem.* **1991**, *34*, 2736.

(9) Momose, T.; Uchida, S.; Kinoshita, M.; Imanishi, T. *Chem. Pharm. Bull.* **1977**, *25*, 1797.

(10) Pitner, J. B.; Abraham, P.; Joo, Y. J.; Triggle, D. J.; Carroll, F. I. *J. Chem. Soc., Perkin Trans. 1* **1991**, 1375.

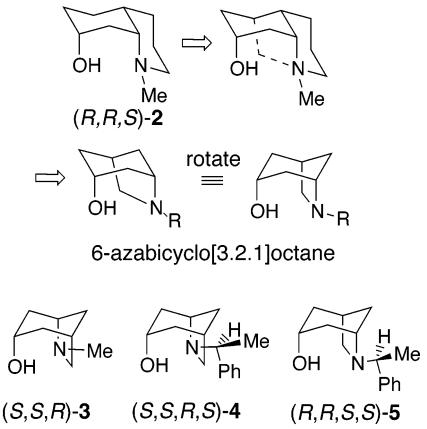


**FIGURE 3.** Development of constrained analogues of **2**.

**TABLE 1. Enantioselective Alkylation of Benzaldehyde Catalyzed by 1−5**[a]

| entry | solvent | R | ligand[b] (L*) | er (*R*):(*S*) | conv (%) |
|---|---|---|---|---|---|
| 1 | $PhCH_3$ | Me | **1** | 48:52 | 29 |
| 2 | 42% THF/$PhCH_3$ | Me | **1** | 62:38 | 7 |
| 3 | $PhCH_3$ | Me | **2** | 73:27 | 51 |
| 4 | 42% THF/$PhCH_3$ | Me | **2** | 85:15 | 33 |
| 5 | $PhCH_3$ | Et | **1** | 47:53 | 94 |
| 6 | 42% THF/$PhCH_3$ | Et | **1** | 61:39 | 18 |
| 7 | $PhCH_3$ | Et | **2** | 73:27 | 87 |
| 8 | 10% THF/$PhCH_3$ | Et | **2** | 84:16 | 50 |
| 9 | 25% THF/$PhCH_3$ | Et | **2** | 84:16 | 30 |
| 10 | 42% THF/$PhCH_3$ | Et | **2** | 84:16 | 32 |
| 11 | 50% THF/$PhCH_3$ | Et | **2** | 86:14 | 18 |
| 12 | 90% THF/$PhCH_3$ | Et | **2** | 86:14 | 16 |
| 13 | $PhCH_3$ | Et | **3** | 67:33 | 36 |
| 14 | $PhCH_3$ | Et | **4** | 53:47 | 59 |
| 15 | $PhCH_3$ | Et | **5** | 63:37 | 31 |

[a] Reaction conditions: After $Et_2Zn$ (1.4 mmol) and ligand (5 mol %) were mixed 30 min at room temperature, PhCHO (1 mmol) was added, and the reaction was halted after 8 h. The enantiomeric ratio and conversion was measured by GC (Cylcodex $\beta$). [b] (*R*,*S*,*S*)-**1** and (*R*,*R*,*S*)-**2** were employed.

high levels of enantioselectivity for **2**, compounds **1**−**2** and constrained analogues **3**−**5** were investigated in the asymmetric addition of dimethyl- and diethylzinc to benzaldehyde. The results are collected in Table 1.

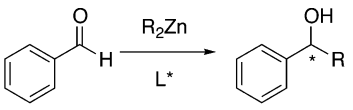


Ligand **2** gave the highest enantioselectivity of 68% ee (entry 8) when THF was used as a cosolvent. Numerous reports indicate that the enantioselectivity of dialkylzinc additions is often influenced by solvent. Typically, noncoordinating solvents (i.e., toluene) provide the best results while the addition of coordinating solvents such as THF decrease the selectivity.[11] The enhancement of selectivities in THF for **1** and **2** is thus unusual and does not appear to be a medium effect (i.e., dielectric) since even small amounts of THF cause a dramatic change (entries 8−12).

The low to moderate enantioselectivity could be attributed to low energy differences between the diastereomeric reaction pathways of **1** and **2**. Alternatively the conformational flexibility of these compounds may give rise to multiple reactive species (Figure 4). From prior work, compounds **1** and **2** were known to predominantly occupy the N-in form in nonpolar media due to hydrogen bonding.[12] As such, we expected the addition of $Et_2Zn$ would lead to predominantly **1-in-Zn** and **2-in-Zn** due to strong metal coordination with the nitrogen and oxygen heteroatoms. Attempts to observe the formation of **1-in-Zn** (Figure 4) by NMR spectroscopy upon addition of 1 equiv of $Et_2Zn$ to **1** at 250 K produces complex spectra which may reflect a dimer−monomer equilibrium as well as competing zinc species (**1-in-Zn** and **1-out-Zn**).

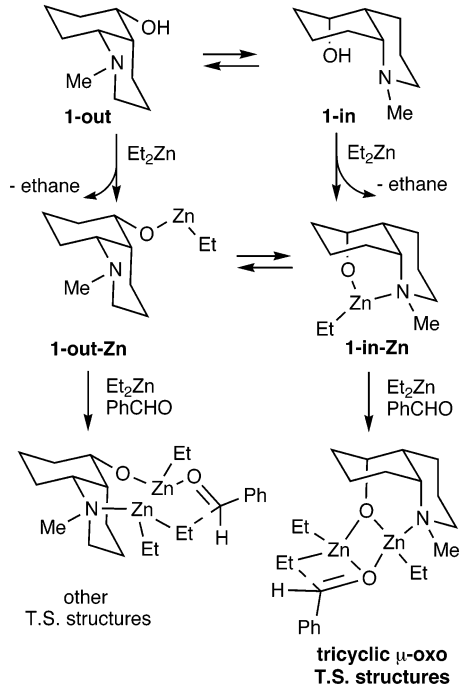


**FIGURE 4.** Schematic of the complexation of **1** with $Et_2Zn$ and benzaldehyde.

Although **2** provides better enantioselection than **1**, the origin of the improved selectivity was not clear. We had previously measured the conformational equilibria of **1** and **2** and found that, in general, the equilibrium ratio of **2-in**/**2-out** (12:1) is higher than **1-in**/**1-out** (2.4:1) in $CDCl_3$ at 240 K.[12] Thus, **2** may give rise to higher enantioselection, because more of **2-in-Zn** is present. Alternatively, structural features of **2** may contribute to a more selective process by stabilization/destabilization of one diastereomeric pathway.

To assess the impact of conformational flexibility on **2**, a constrained analogue (**3**) was designed and synthesized. On this basis, (*S*,*S*,*R*)-**3** would be expected to give the (*S*) product but instead provided the (*R*) product (entry 13, Table 1). In addition, **3** is a less selective ligand than **2**. Surprisingly, the incorporation of *N*-alkyl groups with additional stereogenic centers (**4**, **5**) in place of the *N*-methyl group of **3** did not improve the selectivity (entries 14 and 15, Table 1). Since we had expected the conformationally less flexible **3** to be more selective than **2**, we undertook further calculations of the transition

(11) For specific cases involving THF see ref 17 and Zhang, F.-Y.; Yip, C.-W.; Cao, R.; Chan, A. S. C. *Tetrahedron: Asymmetry* **1997**, *8*, 585.

(12) Phuan, P.-W.; Kozlowski, M. C. *J. Org. Chem.* **2002**, *67*, 6339.

structures of **1**−**3** to understand these experimental results.

**Computational Methods Used in the Transition Structure Calculations.** The presence of two Zn atoms along with the relatively large molecular framework of most ligands employed in these reactions makes the use of high level ab initio methods costly. To our knowledge, most of the theoretical analyses reported so far involve semiempirical methods, combined quantum mechanics−molecular mechanics (QM/MM) methods, or ab initio calculations on model systems. While it is not always possible to choose suitable model systems, semiempirical and QM/MM calculations may not properly consider all the electronic and steric factors relevant to the enantioselectivity. Indeed, initial PM3 transition structure calculations with **2** predicted high selectivity, which stimulated us to examine these compounds. In this study, the relatively small size of ligands **1**, **2**, and **3** enabled us to carry out the calculations at higher levels of theory, which avoids the limitations with semiempirical and QM/MM methods.

All the transition structures for the asymmetric dimethylzinc[13] addition to benzaldehyde catalyzed by ligands **1**, **2**, and **3** were fully optimized using the Hartree-Fock (HF)/LanL2DZ[14] method. The transition structures were located using the synchronous transit-guided quasi-Newton (STQN) method. The guess transition structure geometries were taken from PM3 calculations.[15] The fully optimized transition structures were characterized by one imaginary frequency which corresponds to the migration of the suitably oriented methyl group to the carbonyl carbon. Single point energy calculations were accomplished using B3LYP and MP2 to account for electron correlation. All the calculations were executed using Gaussian 98.[16] Both tricyclic and bicyclic transition structures were traced. The relative energies obtained from the MP2 calculations are invoked in the discussion below unless otherwise noted.

The finding by Noyori et al. that the reaction requires two zinc species per aldehyde[17] led to transition structure models where two Zn atoms are present in different coordination spheres. The $\mu$-oxo tricyclic transition structure models described by Noyori et al.[6a] explain the observed absolute configuration as well as the level of stereoselection in many of the cases. With $\gamma$-amino alcohols as the ligands, the corresponding tricyclic transition structure is composed of a fused 6/4/4 ring system. The four low-energy diastereomeric transition structures are illustrated in Scheme 4: *anti R* (the two unreacting Me groups on the Zn atoms are *anti*, gives (*R*) alcohol), *anti S* (gives (*S*) alcohol), *syn R* (the two unreacting Me groups are *syn* and give (*R*) alcohol), and *syn S*.

**SCHEME 4. Tricyclic *anti* and *syn* $\mu$-Oxo Tricyclic Transition Structures**

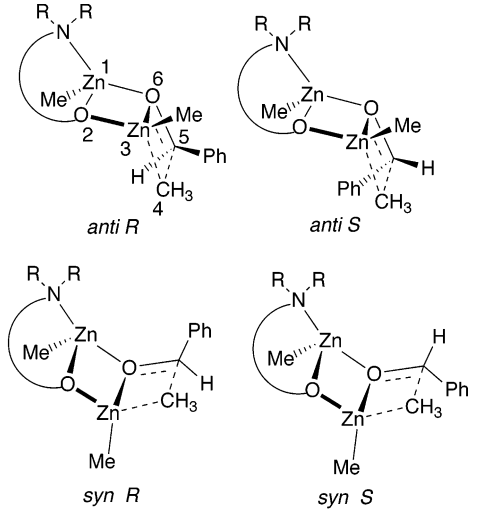


**SCHEME 5. Six-Membered Transition Structures**

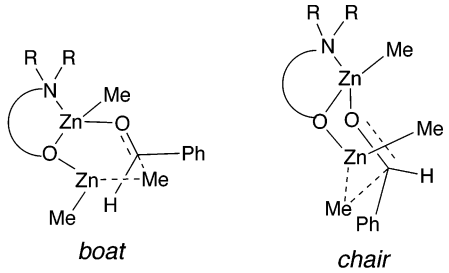


Recently, Norrby et al.[18] characterized bicyclic six-membered transition structures of model systems using B3LYP in conjunction with a higher basis set. The six-membered bicyclic transition structures have one of the Zn atoms in a trigonal planar arrangement, and the aldehydic oxygen is coordinated to only one Zn atom (Scheme 5). For the $\gamma$-amino alcohols, we refer to these transition structures as 6/6. In the sections below, the transition structures for ligands **1**−**3** using HF, density-functional theory (DFT), and MP2 are described and compared with the observed enantioselectivity.

**Transition Structures for Ligand 1.** In the *anti* transition structures (*anti R* and *anti S*) the two unreacting Me groups attached to Zn1 and Zn3 are *anti*, thus the six-membered ring formed by the ligand with Zn1 is *anti* to the Zn3−C4−C5−O6 four-membered ring (Figure 5). The most stable TS for **1** is *anti R*. The next most stable TS, *anti S*, is 1.5 kcal/mol higher in energy due to a steric interaction between phenyl ring and one of the unreacting Me groups (Scheme 4, Figure 5, Table 2). The two four-membered rings (Zn1−O2−Zn3−O6 and Zn3−C4−C5−O6) are distorted to nullify this repulsion. In *anti*

(13) Transition structure calculations used dimethylzinc, which simplifies the computational effort by avoiding the introduction of alkyl rotamers.

(14) LanL2DZ denotes Los Almos effective core potential and double-$\zeta$ basis set for zinc and Dunning−Huzinaga double-$\zeta$ basis set for other atoms.

(15) See Supporting Information for a full discussion.

(16) Frisch, M. J.; Trucks, G. W.; Schlegel, H. B.; Scuseria, G. E.; Robb, M. A.; Cheeseman, J. R.; Zakrzewski, V. G.; Montgomery, J. A., Jr.; Stratmann, R. E.; Burant, J. C.; Dapprich, S.; Millam, J. M.; Daniels, A. D.; Kudin, K. N.; Strain, M. C.; Farkas, O.; Tomasi, J.; Barone, V.; Cossi, M.; Cammi, R.; Mennucci, B.; Pomelli, C.; Adamo, C.; Clifford, S.; Ochterski, J.; Petersson, G. A.; Ayala, P. Y.; Cui, Q.; Morokuma, K.; Malick, D. K.; Rabuck, A. D.; Raghavachari, K.; Foresman, J. B.; Cioslowski, J.; Ortiz, J. V.; Stefanov, B. B.; Liu, G.; Liashenko, A.; Piskorz, P.; Komaromi, I.; Gomperts, R.; Martin, R. L.; Fox, D. J.; Keith, T.; Al-Laham, M. A.; Peng, C. Y.; Nanayakkara, A.; Gonzalez, C.; Challacombe, M.; Gill, P. M. W.; Johnson, B. G.; Chen, W.; Wong, M. W.; Andres, J. L.; Head-Gordon, M.; Replogle, E. S.; Pople, J. A. *Gaussian 98*, revision A.9; Gaussian, Inc.: Pittsburgh, PA, 1998.

(17) Kitamura, M.; Suga, S.; Kawai, K.; Noyori, R. *J. Am. Chem. Soc.* **1986**, *108*, 6071.

(18) Rasmussen, T.; Norrby, P.-O. *J. Am. Chem. Soc.* **2001**, *123*, 2464.

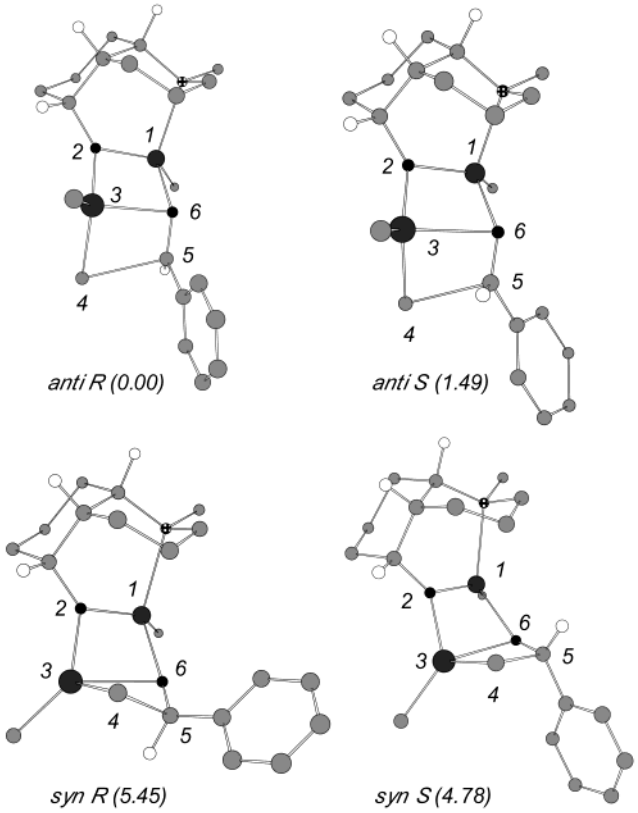


**FIGURE 5.** HF/LanL2DZ optimized geometries of the transition structures with the ligand **1**. Relative MP2 energies (kcal/mol) are given in the parentheses. For clarity, only the hydrogens at stereogenic centers are shown.

*R*, the Zn3−C4 bond of the migrating Me group is parallel to the C═O leading to an almost planar four-membered ring. In contrast, the Zn3−C4 bond of the *anti S* migrating Me group and the C═O bond are twisted about 40°, leading to a nonplanar four-membered ring (Figure 5, *anti S*). The Zn3−O6 bond in *anti S* (2.540 Å) is longer than that of *anti R* (2.332 Å), and the C4−C5 (migrating Me group) is shorter in *anti S* (2.277 Å) than in *anti R* (2.341 Å). These distortions account for the higher energy of *anti S*.

In the *syn S* and *syn R* transition structures, the two unreacting Me groups attached to the Zn atoms are *syn*. Consequently, the six-membered ring formed by the ligand when chelated to Zn1 is *syn* to Zn3−C4−C5−O6 four-membered ring. This forces the substrate closer to the ligand. As a result the *syn* transition structures are 4−5 kcal/mol higher in energy than the *anti* structures. To reduce the severe steric interaction between the ligand and the benzaldehyde substrate in the *syn* transition structures, the Zn1−O6−C5 bond angle becomes wider compared to *anti* structures (*anti R*, 120°; *anti S*, 139°; *syn S*, 149°; *syn R*, 166°). While the phenyl ring avoids the Zn3 Me group in both *syn* transition structures, the proximity of the *syn R* phenyl group to the ligand raises the *syn R* energy 0.8 kcal/mol compared to *syn S*.

The energy difference (1.5 kcal/mol, MP2) between the two diastereomeric transition structures *anti R* and *anti S* would indicate that this ligand should induce some degree of enantioselectivity in the reaction, albeit not as high as DAIB (3.0 kcal/mol, B3LYP).[6b]

**Transition Structures for Ligand 2.** As in **1**, the *anti R* transition structure for **2** is more stable than *anti S* (Figure 6, Table 2). Interestingly, the energy difference is also about the same (1.5 kcal/mol). Again, this is attributed, in part, to the cis arrangement of the phenyl and the Zn1−Me group. The Zn1−O6−C5 angle is wider in *anti S* (141°) than in *anti R* (122°). Thus, the Zn3−C4−C5−O6 four-membered ring is puckered, the Zn3−O6 bond length (2.466 Å) is longer, and the C4−C5 bond is shorter (2.289 Å) compared to those in *anti R* (2.309 and 2.343 Å, respectively).

The *syn* transition structures for **2** reveal similar structural as well as energetic (4−5 kcal/mol higher in energy than their *anti* analogues) trends as **1**. The Zn1−O6−C5 angles in the *syn* are wider (*syn S*, 146°; *syn R*, 159°) than the *anti* (*anti R*, 122°; *anti S*, 141°). In *syn R*, the phenyl is closer to the ligand *N*-Me group, raising its energy by 0.9 kcal/mol compared to *syn S*.

On the basis of the similarity in the relative stabilities of the *anti R* and *anti S* transition structures containing **1** and **2,** we would anticipate that both the ligands should exhibit similar enantioselectivity.

**Transition Structures for Ligand 3.** For **3**, *anti R* is once again the most stable transition structure followed by *anti S* (Figure 7, Table 2). The geometrical features of the transition structures for **3** are similar to those of **1** and **2**. However, the steric distortions are smaller as we go from lower to higher energy transition structures.

The striking difference in this case is the smaller relative energy difference between the transition structures compared to those of **1** and **2**. The *anti S* is only 0.4 kcal/mol higher in energy than *anti R*. The *syn R* and *syn S* possess almost the same energy and are 3.7 kcal/mol higher in energy than the most stable *anti R*. On this basis, we would expect **3** to be less selective than **1** or **2**.

The three different methods (HF, B3LYP, and MP2) employed in this study revealed identical trends (Table 2). For all the cases studied [(*R*,*S*,*S*)-**1**, (*R*,*R*,*S*)-**2,** and (*S*,*S*,*R*)-**3**], the *anti R* transition structure which leads to the (*R*) alcohol is found to be the most stable transition structure at each level of theory. The different theoretical methods predict the *anti S* transition structure to be the next most stable.

**6/6 Transition Structures.** Norrby et al. reported that the PM3 bicyclic transition structures for certain $\beta$-amino alcohols are lower in energy than the tricyclic structures. We had also located the 6/6 bicyclic transition structures at the PM3 level[19] for $\gamma$-amino alcohols, **1**−**3**. These PM3 structures are 4−8 kcal/mol lower in energy compared to their 6/4/4 analogues.

To determine if these transition structures are relevant to this case, we carried out HF/LanL2DZ optimizations of the 6/6 transition structures for **3**. Two 6/6 transition structures, *twist boat R* and *boat S*, were located (Figure 8). In both, the methyl group migrates with retention of configuration in a manner similar to the bicyclic transi-

(19) We independently located the 6/6 transition structures for the ligands **1**−**3,** similar to those reported by Norrby et al. in ref 18, while locating the different possible 6/4/4 transition structures at the PM3 level (see Supporting Information). The PM3 calculations were done using SPARTAN version 5.0. Wavefunction, Inc., 18401 Von Karman Avenue, Suite 370, Irvine, CA 92612.

**TABLE 2. Total Energies (Hartrees) and Relative Energies (in Parentheses; kcal/mol) of the Tricyclic Diastereomeric Transition Structures for the Ligands 1−3 and Bicyclic Ones for 3 from ab initio and DFT Calculations (LanL2DZ Basis Set Used Throughout)**

| | HF//HF | B3LYP//HF | MP2//HF |
|---|---|---|---|
| | | **1** | |
| *anti R* | −1107.51724 (**0.00**) | −1118.26217 (**0.00**) | −1109.99443 (**0.00**) |
| *anti S* | −1107.51277 (**2.80**) | −1118.25879 (**2.12**) | −1109.99205 (**1.49**) |
| *syn R* | −1107.50814 (5.71) | −1118.25477 (4.64) | −1109.98574 (5.45) |
| *syn* S | −1107.51166 (3.45) | −1118.25716 (3.14) | −1109.98681 (4.78) |
| | | **2** | |
| *anti R* | −1107.52172 (**0.00**) | −1118.26609 (**0.00**) | −1109.99640 (**0.00**) |
| *anti S* | −1107.51735 (**2.74**) | −1118.26305 (**1.91**) | −1109.99402 (**1.49**) |
| *syn R* | −1107.51149 (6.42) | −1118.25759 (6.31) | −1109.98635 (5.33) |
| *syn* S | −1107.51634 (3.37) | −1118.26119 (3.06) | −1109.98940 (4.44) |
| | | **3** | |
| *anti R* | −1029.47038 (**0.00**) | −1039.64436 (**0.00**) | −1031.76558 (**0.00**) |
| *anti S* | −1029.46786 (**1.58**) | −1039.64251 (**1.16**) | −1031.76448 (**0.44**) |
| *syn R* | −1029.46438 (3.76) | −1039.63893 (3.41) | −1031.75969 (3.70) |
| *syn* S | −1029.46658 (2.38) | −1039.64035 (2.52) | −1031.75962 (3.74) |
| | | **3** (6/6) | |
| twist boat *R* | −1029.45914 (**7.05**) | −1039.63584 (**5.35**) | −1031.75774 (**4.92**) |
| boat *S* | −1029.46588 (**2.82**) | −1039.64110 (**2.04**) | −1031.76419 (**0.87**) |

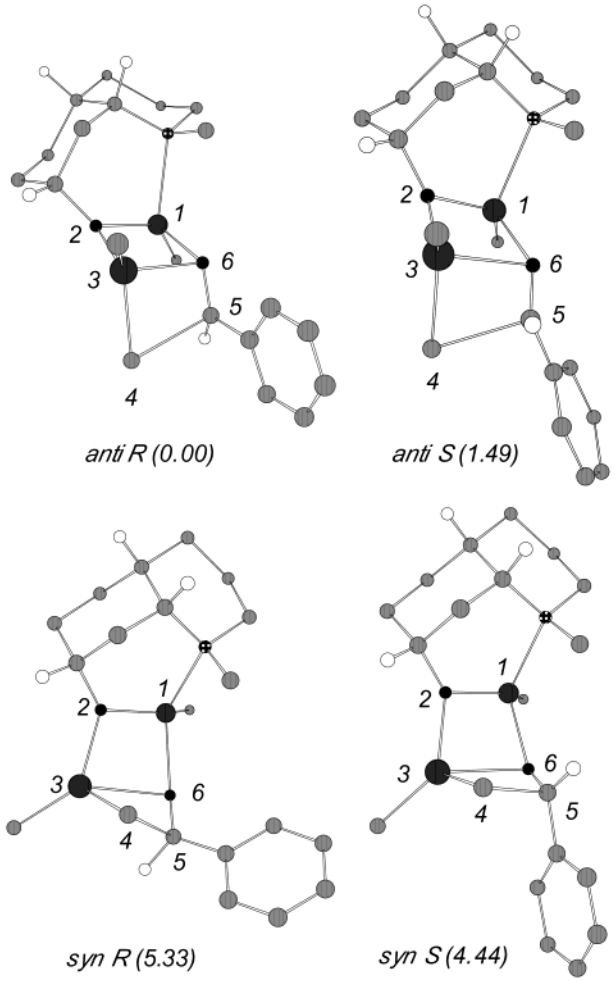


**FIGURE 6.** HF/LanL2DZ optimized geometries of the transition structures with the ligand **2**. Relative MP2 energies (kcal/mol) are given in the parentheses. For clarity, only the hydrogens at stereogenic centers are shown.

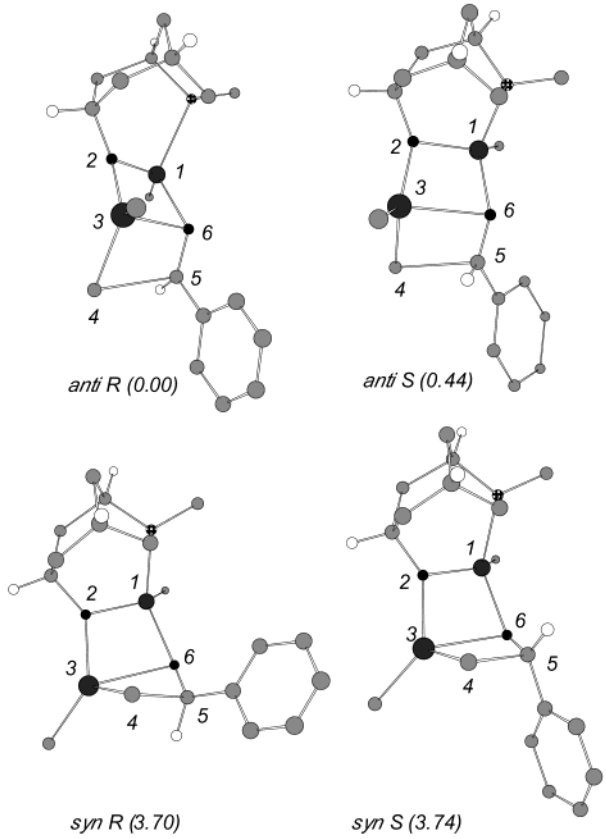


**FIGURE 7.** HF/LanL2DZ optimized geometries of the transition structures with the ligand **3**. Relative MP2 energies (kcal/mol) are given in the parentheses. For clarity, only the hydrogens at stereogenic centers are shown.

tion structures identified by Norrby. The chair transition structure described by Norrby was not a saddlepoint for these systems due to steric interactions with the chiral ligand. The most significant geometrical change between the 6/4/4 and 6/6 transition structures occurs at the Zn3 atom which becomes trigonal planar and no longer coordinates the carbonyl oxygen.

In the HF/LanL2DZ calculations, the 6/6 transition structures were found to be higher in energy than their 6/4/4 analogues (Table 2). In addition, the *boat S* transi-

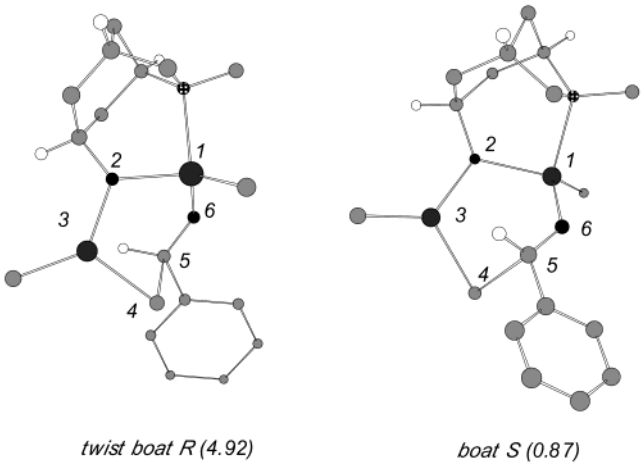


**FIGURE 8.** HF/LanL2DZ optimized geometries of the 6/6 transition structures leading to (*R*) and (*S*) products using the ligand **3**. The relative energies (kcal/mol) with respect to the most stable 6/4/4 transition structure at the MP2 level are given in parentheses.

**TABLE 3. Comparison of the Calculated Results with the Experimental Data**[a]

| | calculated (MP2//HF) | | |
|---|---|---|---|
| | $\Delta E$ (kcal/mol) | ee (%) | exp ee (%) |
| **1** | 1.49 | 85 (*R*) | 4 (*S*) |
| **2** | 1.49 | 85 (*R*) | 46 (*R*) |
| **3** | 0.44 | 35 (*R*) | 34 (*R*) |

[a] $\Delta E$ is the energy difference between the two lower energy transition structures giving (*R*) and (*S*) alcohols. Calculated enantiomeric excess is obtained from a Boltzmann distribution of the transition structures at 298 K.

tion structure is lower in energy compared to *twist boat R*, which predicts the (*S*) alcohol as the dominant product for **3** in contrast to the experimental finding. These results imply that the 6/6 transition structures are not playing a major role in the reactions of these $\gamma$-amino alcohol ligands.

**Comparison of the Calculated and Experimental Data for Ligands 1−3.** For the DAIB ligand which gives very high enantioselectivity (95% ee), a 3.5 kcal/mol energy difference between the two lowest energy transition structures leading to the (*R*) and (*S*) products was reported by Yamakawa and Noyori[6a] from B3LYP calculations using a basis set similar to the one employed here. For the ligands **1**, **2,** and **3**, we found smaller energy differences of 2.1, 1.9, and 1.2 kcal/mol, respectively, using B3LYP calculations. The MP2//HF results reveals even smaller energy differences (1.5 kcal/mol for **1** and **2,** and 0.4 kcal/mol for **3**). Thus, these calculations predict that our ligands would be less selective than DAIB. In toluene, the diethylzinc addition to benzaldehyde catalyzed by **1**, **2**, and **3** give enantiomeric excesses of 4% (*S*), 46% (*R*), and 34% (*R*), respectively. Qualitatively, the calculated selectivities match the observed sense of stereoselection, except for the case of **1**, which provides a minor selectivity (4% ee) for the (*S*) alcohol (Table 3). From **2** to **3,** the energy difference between *anti R* and *anti S* transition structures decreases by 1.1 kcal/mol. This general trend is qualitatively consistent with the experimental 12% ee decrease from **2** to **3**.

Formation of six-membered chelates between the $\gamma$-amino alcohols and zinc places the benzaldehyde substrate further from the ligand compared to the $\beta$-amino alcohols, which form five-membered chelates. Thus, the steric effects offered by the ligand substituents in **1**−**3** are reduced, resulting in lower enantioselectivity. These ligands also differ from many of the successful $\beta$-amino alcohols, in that they lack bulky substituents on the carbons adjacent to the nitrogen and oxygen. As a result, there are smaller repulsive interactions between the chiral catalysts and the substrates.

On the basis of prior results and the results from conformationally restricted **3** which match the calculations very well (Table 3), it appears reasonable that transition structure calculations can be a predictive tool for estimating reaction enantioselectivity. The discrepancy between the calculated results and the experimental data for **1** and **2** most likely arises from the intervention of other ligand−metal species due to the conformationally flexible nature of **1** and **2** (see Figure 4). These results indicate that caution must be exercised in the design of new systems, since the presence of other species which may be or may not be catalytically relevant can alter the basic reaction paradigm.

## Concluding Remarks

We have synthesized, resolved, and examined $\gamma$-amino alcohols **1**−**5** in the asymmetric organozinc addition to benzaldehyde. While preliminary PM3 calculations had predicted that **2** would be highly selective, we observed only moderate selectivity. Thus, the origin of the enantioselectivity for $\gamma$-amino alcohols **1**−**3** was explored using higher level quantum calculations. The calculations predict that the (*R*) alcohol should be the predominant product for all the three ligands. Results from **2** and **3** agree with this trend, whereas those from **1** do not. The 12% ee decrease from **2** to **3** is also reflected in the calculations. Thus, the MP2//HF method can be useful in estimating the relative selectivity of these $\gamma$-amino alcohols.

The low enantioselectivities for these ligands may be attributed to two factors. First, the energy difference between the two lowest energy transition structures to the enantiomeric products is smaller compared to other highly selective ligands. For instance, the energy difference between the two lowest energy transition structures incorporating DAIB[6b] is about twice that of **1**, **2**, and **3**. Second, the conformational flexibility of **1** and **2** appears to give rise to other catalytic ligand−zinc species with transition structures (Figure 4) different than the $\mu$-oxo tricyclic structures used in the calculations.

While 6/6 transition structures may be low-energy pathways in some systems, they were found to be higher in energy than the 6/4/4 transition structures for **1**−**3** when HF, DFT, and MP2 methods were employed. The 6/6 transition structure of **3** leading to (*S*) product is also lower in energy than that corresponding to the (*R*) product (in contrast to experiment), which further contraindicates the intervention of the 6/6 transition structures for these ligands.

Overall, we have found that PM3 calculations are not reliable for anticipating the selectivity in asymmetric alkylation of amino alcohol catalysts which diverge from

the $\beta$-amino alcohol framework. Among the quantum chemical calculations examined (HF, DFT, MP2), MP2 proved most useful in estimating the selectivity for the $\gamma$-amino alcohols. Even so, caution must be employed in the calculations of conformationally flexible amino alcohols, as other catalyst forms may intervene.

**Acknowledgment.** Financial support was provided by the National Institutes of Health (GM-59945) and Merck Research Laboratories. Acknowledgment is made to the donors of the Petroleum Research Fund, administered by the American Chemical Society, for partial support of this research. We thank Dr. Bishwajit Ganguly for performing the initial PM3 6/4/4 transition structure calculations with **1**−**2**. Computational support was provided by the NCSA in the form of a supercomputing time allotment. The invaluable assistance of Dr. George Furst in collecting the NMR spectroscopic data and of Dr. Patrick Carroll in obtaining the X-ray structures is gratefully acknowledged.

**Supporting Information Available:** Full experimental details and characterization, X-ray structure methods and data tables for **13** and **14**, results from PM3 calculations along with the coordinates for the HF transition structures, and geometries of the transition structures at HF/LanL2DZ. This material is available free of charge via the Internet at http://pubs.acs.org.

JO0262210